Available online at www.eccomasproceedia.org
Eccomas Proceedia UNCECOMP (2025) 383-390

ECCOMAS Proceedia

UNCECOMP 2025
6th ECCOMAS Thematic Conference on
Uncertainty Quantification in Computational Science and Engineering
M. Papadrakakis, V. Papadopoulos, G. Stefanou (eds.)
Rhodes Island, Greece, 15-18 June 2025

MULTISCALE STRUCTURAL OPTIMIZATION WITH EMBEDDED HIERARCHICAL MATERIAL ARCHITECTURES

Andrea Chiozzi[1] and Andrea Nale[2]

[1] University of Ferrara, Department of Environmental and Prevention Sciences
Via Ercole I d'Este 32, 44121 Ferrara, Italy
e-mail: andrea.chiozzi@unife.it

[2] University of Ferrara, Department of Architecture
Via della Ghiara 36, 44121 Ferrara, Italy
e-mail: andrea.nale@unife.it

Abstract. *Traditional topology optimization techniques enable the development of structurally efficient designs subject to specific constraints, loads, and boundary conditions. These methods typically involve continuous modifications of the topology throughout the optimization process. In this work, we introduce an innovative multiscale structural optimization framework, based on the minimization of compliance, that decouples design across scales: the microscale topology is optimized using a multi-material strategy, while the macroscale geometry of the domain remains fixed. This formulation takes advantage of embedding optimized hierarchical material architectures at the microscale, thereby enabling exploration across a broad range of structural configurations. Meaningful numerical examples are provided to demonstrate the capabilities and relevance of the proposed method.*

Keywords: Multiscale structural optimization, topology optimization, architected materials, homogenization, additive manufacturing

Peer-review under responsibility of the organizing committee of UNCECOMP 2025.
doi: 10.7712/120225.12363.21463

1 INTRODUCTION

Topology optimization is a computational design methodology used to determine the most efficien material layout within a define domain, based on specifi boundary conditions and loading scenarios, while optimizing a particular objective under given constraints. Historically, research in this area focused largely on theoretical developments due to the difficult in manufacturing the complex geometries produced by these methods. However, with the advent of advanced manufacturing technologies, particularly 3D printing, many of these limitations have been mitigated. This progress has enabled the application of topology optimization across various engineering disciplines, including automotive, aerospace, and biomedical sectors.

The shift from traditional manufacturing to additive manufacturing (AM) has also opened new opportunities in industry. The motivation for this transition is driven by the need to reduce the environmental footprint and lower production costs. Integrating topology optimization with AM is therefore seen as a signifi ant advancement, as it promotes energy efficien y and reduces carbon emissions. Topology optimization helps achieve material efficien y by designing structures that use the minimum necessary material, following the principle of "limits of economy" [1]. Concurrently, AM minimizes waste and supports the use of sustainable and recycled materials, such as natural aggregates combined with environmentally friendly binders.

The synergy between AM and topology optimization has encouraged exploration into structural design across multiple scales. Control at the microscale has enabled the development of lightweight cellular materials with tailored properties at the macroscale. Nevertheless, common periodic microstructures, such as truss or plate-based designs, often suffer from stress concentrations at junctions, affecting their strength and reliability.

An effective alternative is found in triply periodic minimal surfaces (TPMS) [2], which avoid stress concentrations through smooth geometries and offer superior scalability thanks to their doubly curved surfaces. More recently, attention has shifted to non-periodic stochastic structures inspired by spinodal decomposition processes during phase separation. These spinodal architectures also exhibit smooth, non-intersecting interfaces between material phases, akin to TPMS [3].

In this study, we introduce a volume-constrained, multiscale, multi-material topology optimization framework aimed at maximizing structural stiffness by optimally distributing various types of material architectures with different densities and orientations [4], such as TPMS [5] or spinodal architectures [6]. This framework can be integrated with large-scale additive manufacturing using a voxel-based post-processing approach [6].

This paper is structured as follows: Section 2 presents the optimization formulation, the characteristics of non-periodic architected materials, and the applied additive manufacturing techniques. Section 3 discusses numerical results, and Section 4 concludes with fina thoughts and directions for future research.

2 MATERIALS AND METHODS

The presented topology optimization framework adopts a multi-material strategy grounded in homogenization, enabling the integration and manipulation of various microstructures throughout the iterative design process. As define in Eq. 1, the objective is to minimize structural compliance, J, while satisfying a set of volume constraints, g_k.

$$
\begin{aligned}
\min_{\mathbf{Z},\rho,\alpha,\beta,\gamma} \quad & J = \mathbf{F}^T\,\mathbf{U}(\mathbf{Z},\rho,\boldsymbol{\alpha},\boldsymbol{\beta},\boldsymbol{\gamma}), \\
\text{s.t.} \quad & g_k = \frac{\sum_{m\in\mathcal{G}_k}\sum_{\ell\in\mathcal{E}_j} A_\ell m_v(y_{\ell m})}{\sum_{\ell\in\mathcal{E}_k} A_\ell} - \overline{v}_k \le 0,\ k = 1,\dots,N^{\mathrm{c}}, \\
& Z_{\ell m} \in [0,1],\ \ell = 1,\dots,N^{\mathrm{el}},\ m = 1,\dots,N^{\mathrm{mat}}, \\
& \rho_\ell \in [\underline{\rho},\overline{\rho}],\ \{\alpha_{\ell m},\beta_{\ell m},\gamma_{\ell m}\} \in [-\pi,\pi], \\
\text{with} \quad & \mathbf{K}(\mathbf{Z},\rho,\boldsymbol{\alpha},\boldsymbol{\beta},\boldsymbol{\gamma})\,\mathbf{U}(\mathbf{Z},\rho,\boldsymbol{\alpha},\boldsymbol{\beta},\boldsymbol{\gamma}) = \mathbf{F},
\end{aligned}
\tag{1}
$$

The volume constraint is define with fl xibility, allowing for either global or localized material limitations. Local constraints are implemented by restricting material choices within specifi subdomains, identifie through lists of element indices. Specificall , each material index list, $\mathcal{G}k$, specifie the materials permitted during optimization, and is associated with an element index list, $\mathcal{E}k$. For global constraints, $\mathcal{E}_k$ refers to the entire domain, whereas for local constraints, it targets define subdomains. Additionally, passive regions can be designated within the domain—these can either be voids or regions composed of a specifi material, referred to respectively as passive-void and passive-solid zones.
The design variable space includes material presence $\mathbf{Z}$, spinodal density $\boldsymbol{\rho}$—bounded between $\underline{\rho}$ and $\overline{\rho}$ to ensure manufacturability—and spinodal orientation angles $\boldsymbol{\alpha},\boldsymbol{\beta},\boldsymbol{\gamma}$. The material distribution fiel $\mathbf{Z}$ is regularized using a linear filte [7], which applies a specifie radius to ensure mesh independence and well-posedness of the optimization problem. To promote distinct material–void transitions, this filte is combined with a Heaviside projection [8]. The resulting filtere density fiel $\tilde{Y}$ is further processed using a SIMP (Solid Isotropic Material with Penalization) interpolation scheme [9] to discourage intermediate density values.
To progressively refin the solution, continuation methods are applied to gradually increase both the material penalization factor p and the material mixing parameter τ until target values are reached, either upon convergence or after a specifie number of iterations. Once the optimal material layout is obtained, the solid boundaries are smoothed appropriately. A post-processing step is then necessary to both visualize and incorporate the designed microstructures.
The computational domain is discretized using finit elements, with each element linked to a corresponding set of design variables. The displacement field $\mathbf{U}$, is calculated by solving the linear elastic equilibrium equation $\mathbf{K}(\mathbf{Z},\boldsymbol{\rho},\boldsymbol{\alpha},\boldsymbol{\beta},\boldsymbol{\gamma}),\mathbf{U}(\mathbf{Z},\boldsymbol{\rho},\boldsymbol{\alpha},\boldsymbol{\beta},\boldsymbol{\gamma}) = \mathbf{F}$, where $\mathbf{F}$ is a prescribed, design-independent vector of nodal forces. The global stiffness matrix $\mathbf{K}$ is assembled from the elemental stiffness contributions [10] as described below:

$$
\mathbf{K}_\ell = \int_{\Omega_\ell} \mathbf{B}^T\mathbf{D}_\ell(\mathbf{Z}_\ell,\rho_\ell,\boldsymbol{\alpha}_\ell,\boldsymbol{\beta}_\ell,\boldsymbol{\gamma}_\ell)\mathbf{B}d\mathbf{x},, \tag{2}
$$

The element-strain displacement matrix is $\mathbf{B}$ and the material matrix, $\mathbf{D}$, is calculated by multi-material interpolation of the m-candidate materials material matrix, D^H_m, according to:

$$
\mathbf{D}_\ell = \sum_{m=1}^{N^m} w_{\ell m} \prod_{\substack{q=1\\ q\neq m}}^{N^m} (1-\tau w_{\ell q})\mathbf{M}(\alpha_{\ell m},\beta_{\ell m},\gamma_{\ell m})\mathbf{D}^H_m(\rho_\ell)\mathbf{M}^T(\alpha_{\ell m},\beta_{\ell m},\gamma_{\ell m}). \tag{3}
$$

The optimal orientation of spinodal architectures reference frame is obtained by tensor transformation laws, $\mathbf{M}(\alpha_{\ell m},\beta_{\ell m},\gamma_{\ell m})$, for stress and strains. The angles $(\alpha_{\ell m},\beta_{\ell m},\gamma_{\ell m})$ are updated by Eq. 6. The m-candidate materials are included by a homogenized material elasticity tensor,

D_m^H, calculated by classical homogenization theory [11] for assigned densities and topologies. The stochastic and non-periodic nature of spinodal topology is considered in the implementation by calculating the elastic tensor by means of 15 spinodal architectures. Each topology is calculated by applying level-set function to Eq. 11 and the computational homogenization is performed by discretizing the topology in 150x150x150 elements with Young's modulus, E = 1, and Poisson's ratio, $\nu = 0.3$ for the bulk material. The problem in Eq. (1) is solved by a gradient-based approach. The optimal solution is ruled by the sensitivities of objective and constraint functions with respect to design variables. The augmented lagrangian method [12] is adopted with the Steepest Descent Method (SDM) [13] to iteratively guide the design toward an optimal solution, a local minimum. The augmented lagrangian function is minimized in each inner iteration t as the sum of objective function and the penalty term and reads:

$$\mathcal{L}(\mathbf{x})^{(\mathbf{t})} = J(\mathbf{x}) + \sum_{j=1}^{K}\left[\lambda_j^{(t)} \max\left(g_j(x), -\frac{\lambda_j^{(t)}}{\mu^{(t)}}\right) + \frac{\mu^{(t)}}{2} max\left(g_j(x), -\frac{\lambda_j^{(t)}}{\mu^{(t)}}\right)^2\right], \tag{4}$$

The penalization parameters, $\lambda_j^{(k)}$ and $\mu^{(k)}$, are updated every 5 outer iterations, k, as:

$$\lambda_j^{(k+1)} = \lambda_j^{(k)} + \mu^{(k)} \max\left(g_j^{(k)}(\mathbf{x}), -\frac{\lambda_j^{(t)}}{\mu^{(k)}}\right) \; and \; \mu^{(k+1)} = 1.25\mu^{(k)}. \tag{5}$$

At each inner optimization iteration, t, the variables $\mathbf{x}$ are updates following the rule:

$$\mathbf{x}^{(t+1)} = \max\left[\min\left(\mathbf{x}^{(t)} - \tau^{(t)}\frac{\partial \mathcal{L}^{(t)}}{\partial \mathbf{x}}, \mathbf{x}^{(t)} + move\right), \mathbf{x}^{(t)} - move)\right], \tag{6}$$

where $move$ is move limit and $\tau^{(t+1)} = \max\left(0.99\tau^{(t)}, 0.01\right)$ is the step size with $\tau^{(0)} = 1$.
The sensitivities involved in the update scheme are the objective and penalty function and they are computed as follows:

$$\begin{aligned}
&\frac{\partial J}{\partial \mathbf{z}_m} = \frac{\partial y_{\ell m}}{\partial z_{\ell m}}\frac{\partial \tilde{y}_{\ell m}}{\partial y_{\ell m}}\frac{\partial J}{\partial w_{\ell m}}, \; \frac{\partial J}{\partial \boldsymbol{\alpha}_m} = \frac{\partial J}{\partial \alpha_{\ell m}}, \frac{\partial J}{\partial \rho} = \frac{\partial J}{\partial \rho_\ell}\\
&\frac{\partial g_j}{\partial \mathbf{z}_m} = \frac{\partial y_{\ell m}}{\partial z_{\ell m}}\frac{\partial \tilde{y}_{\ell m}}{\partial y_{\ell m}}\frac{\partial v_{\ell m}}{\partial \tilde{y}_{\ell m}}\frac{\partial g_j}{\partial v_{\ell m}}, \; \frac{\partial g_j}{\partial \boldsymbol{\rho}} = \frac{\partial v_{\ell m}}{\partial \rho_\ell}\frac{\partial g_j}{\partial v_{\ell m}},\\
&m = 1, ..., N^m, \; j = 1, ..., N^c
\end{aligned} \tag{7}$$

where:

$$\begin{aligned}
&\frac{\partial y_m}{\partial Z_m} = \mathbf{P}^T, \frac{\partial w}{\partial \tilde{y}_{\ell m}} = p y_{\ell m}^{p-1}, \frac{\partial \tilde{y}}{\partial y_{\ell m}} = \frac{\xi(1 - \tanh^2(\xi(y_{\ell m} - \eta)))}{\tanh(\xi\eta) + \tanh(\xi(1-\eta))},\\
&\frac{\partial v_{\ell m}}{\partial \tilde{y}} = \rho_\ell, \frac{\partial v_{\ell m}}{\partial \rho_k} = \tilde{y}_{\ell m}, \frac{\partial g_j}{\partial v_{\ell m}} = \frac{V_\ell}{\sum_{\ell \in E_j} V_\ell}
\end{aligned} \tag{8}$$

The components of each objective and constraint sensitivities are define as:

$$\frac{\partial J}{\partial w_{\ell m}} = -\mathbf{U}^T\frac{\partial \mathbf{K}}{\partial w_{\ell m}}\mathbf{U}, \; \frac{\partial J}{\partial \rho_\ell} = -\mathbf{U}^T\frac{\partial \mathbf{K}}{\partial \rho_\ell}\mathbf{U}, \frac{\partial J}{\partial \alpha_{\ell m}} = -\mathbf{U}^T\frac{\partial \mathbf{K}}{\partial \alpha_{\ell m}}\mathbf{U} \tag{9}$$

where the stiffness sensitivities are computed from the material elasticity tensor, with respect to the design variable, $\mathbf{w}$, the spinodal density, ρ, and the orientation angle (α):

$$\frac{\partial \mathbf{D}_\ell}{\partial w_{\ell m}} = \prod_{\substack{q=1 \\ q\neq m}}^{N^m} (1-\tau w_{\ell q})\mathbf{M}_{\ell m}\mathbf{D}_m^H(\rho_\ell)\mathbf{M}_{\ell m}^T - \sum_{\substack{q=1 \\ q\neq m}}^{N^m} \gamma w_{\ell q} \prod_{\substack{r=1 \\ r\neq q \\ r\neq m}}^{N^m} (\tau_{\ell r})\mathbf{M}_{\ell m}\mathbf{D}_m^H(\rho_\ell)\mathbf{M}_{\ell m}^T,$$

$$\frac{\partial \mathbf{D}_\ell}{\partial \rho_\ell} = \sum_{m=1}^{N^m} w_{\ell m} \prod_{\substack{q=1 \\ q\neq m}}^{m} (1-\tau w_{\ell q})\mathbf{M}_{\ell m}\frac{\partial \mathbf{D}_m^H(\rho_k)}{\partial \rho_\ell}\mathbf{M}_{\ell m}^T, \tag{10}$$

$$\frac{\partial \mathbf{D}_\ell}{\partial \alpha_{\ell m}} = \sum_{m=1}^{N^m} w_{\ell m} \prod_{\substack{q=1 \\ q\neq m}}^{N^m} (1-\tau w_{\ell q})\left[\frac{\partial \mathbf{M}_{\ell m}}{\partial \alpha_{\ell m}}\mathbf{D}_m^H\mathbf{M}_{\ell m}^T + \mathbf{M}_k\mathbf{D}_m^H\frac{\partial \mathbf{M}_{\ell m}^T}{\partial \alpha_{\ell m}}\right]$$

with $\partial\mathbf{D}/\partial\beta_{\ell m}$ and $\partial\mathbf{D}/\partial\gamma_{\ell m}$ and of similar form.

3 NUMERICAL RESULTS

The optimization formulation described in Eq. 1 is coupled with a homogenization strategy that facilitates the incorporation of microstructural features into the design of multiscale, hierarchical structures. In this work, we adopt spinodal architected materials as the microstructural design basis. These materials derive their topology from the thermodynamic phenomenon of spinodal decomposition [16], wherein a homogeneous phase at peak free energy undergoes spontaneous separation into two distinct phases. This separation is initiated by small fluctua tions in concentration, which lower the system's free energy.

Spinodal decomposition was originally modeled by the Cahn–Hilliard equation [17], which, while accurate, is computationally intensive and offers limited control over the resulting microstructure. To address this, a more practical phase-fiel approximation based on Gaussian random field (GRFs) has been proposed [18].

The introduction of a GRF, ω, sets anisotropic features by manipulating the stochastic distribution of a set of wave vectors, $\mathbf{n}_i, i = 1, ...N^w$, on a unit sphere $\mathbf{n}_i \in \mathcal{U}[\mathbb{S}^2]$. The GRF in the Cartesian space $\mathbb{R}^3$ with basis $\{\hat{\mathbf{e}}_1, \hat{\mathbf{e}}_2, \hat{\mathbf{e}}_3\}$ is computed as follows:

$$\omega(\mathbf{x}) = \sqrt{\frac{2}{N^w}} \sum_{j=1}^{N^w} \cos\beta\mathbf{n}_j \cdot \mathbf{x} + \zeta_j, \tag{11}$$

with amplitude, N^w, wavelength, β and phase shift $\zeta_j \in \mathcal{U}[0, 2\pi)$ of the j-th wave vector sampled as:

$$\mathbf{n}_j \in \mathcal{U}[\{\mathbf{m} \in \mathbb{S}^2 : (|\mathbf{m}\cdot\hat{\mathbf{e}}_1| > \cos\theta_1) \oplus (|\mathbf{m}\cdot\hat{\mathbf{e}}_2| > \cos\theta_2) \oplus (|\mathbf{m}\cdot\hat{\mathbf{e}}_3| > \cos\theta_3)\}], \tag{12}$$

where the angle set $\{\theta_1, \theta_2, \theta_3\} \in [0, \pi/2]$ restricts the wave vectors 12 on an unit sphere [18] providing the desirable anisotropic features.

The numerical model and the physical sample include the lamellar spinodal architecture. The lamellar class is generated by restricting wave vectors through cone angles $\{\theta_1, \theta_2, \theta_3\} = \{0, 30, 0\}$. The homogenized properties are included in the optimization formulation by the elastic matrix D^H.

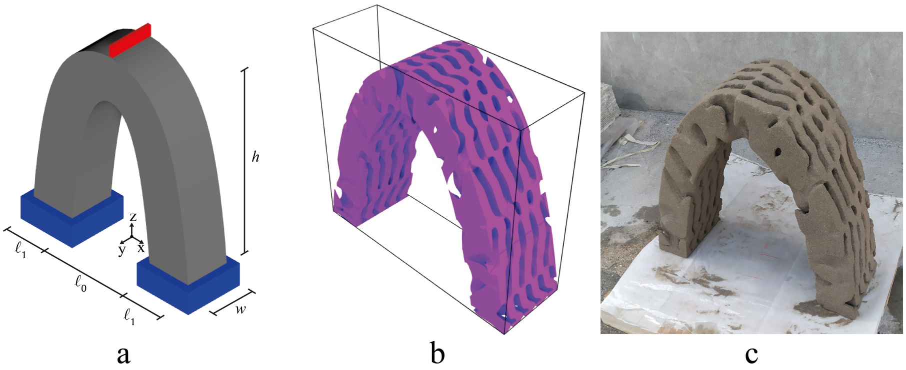

Figure 1 Lamellar Catenary Arch: a) domain, b) numerical model, c) manufactured sample.

The proposed topology optimization framework has been here applied using a single material class; specificall , the lamellar spinodal architecture—subject to a global volume constraint $\overline{v}$. The optimization process focuses on determining the optimal spatial orientation of the microstructure within a 3D domain. The design space is define as a catenary arch, with its geometry and boundary conditions illustrated in Fig. 1. The central axis of the structure follows the inverse of the standard catenary equation: $z = a \cosh(x/a) = a(e^{x/a} + e^{-x/a})/2$. To generate the solid arch, the parameter $a = 1/6$ sets the vertical distance from the lowest point of the arch to the x-axis, while a constant depth of $\ell_1 = 15$ cm is maintained along its axis. The structure spans a length $\ell_0 = 65$ cm, yielding a total length of $\ell = 95$ cm, a height of $h = 83$ cm, and a fi ed width of $w = 30$ cm.

The optimization is initialized by assigning values to the design variables: the material volume is define as $v_{lm} = \overline{v}/\rho_\ell$ for all elements ℓ, with the initial density set to the midpoint value $\rho_\ell = (\underline{\rho} + \overline{\rho})/2$, and all orientation angles initialized as $\alpha_\ell = \beta_\ell = \gamma_\ell = 0$. A linear filte with radius $R = 0.4$ is applied to the density fiel to ensure smooth transitions. The design variables are then iteratively updated according to Eq. 6, with maximum allowable changes of $move_z = 0.1$ for density and $move_{ang} = 0.25$ for orientation angles. Convergence is assessed by monitoring the variation in the density fiel $\mathbf{Z}$ until it falls below a specifie tolerance tol, with each penalization phase limited to $\max^{iter} = 150$ iterations.

The search for an optimal solution is conducted through a continuation scheme involving five stages of penalization, using material penalty values $p = [1, 2, 2, 3, 4]$. Since the formulation involves only one material class, the multi-material interpolation factor τ is not needed. The iterative optimization routine refine the material layout, porosity distribution, and microstructural orientation throughout the domain.

This methodology is specificall adapted for water jetting powder-bed additive manufacturing, which is well-suited for producing self-supporting geometries. Due to the inherent lack of tensile strength in the printed material, the approach favors compression-dominant structural forms. Both simulation results and the fabricated prototype confir the feasibility of using this AM process to construct large-scale components from non-periodic architected materials.

4 CONCLUSIONS

This work demonstrates the scalability of spinodal architectures within a large-scale additive manufacturing context, exemplifie by the fabrication of an optimally oriented lamellar catenary arch. Given the brittle, stone-like nature of the printed materials used—characterized by negligible tensile strength—along with the characteristics of the adopted optimization method, a self-supporting structure was chosen as the design input. Such structures are predominantly subjected to compressive stress, aligning with the material's mechanical behavior. The adopted topology optimization approach does not incorporate any failure criteria. Although stress-based formulations—such as the one proposed in [19]—might be more suitable for practical applications, their integration within multiscale systems remains a significan challenge. Looking ahead, future research will explore the incorporation of failure-based criteria, such as stress-constrained formulations, and the use of many different classes of materials architectures at the microscale.

5 ACKNOWLEDGEMENTS

Andrea Chiozzi gratefully acknowledges the financia support of European Union - Next Generation EU, Italian Ministry of University and Research (MUR) under the program "Progetti di Ricerca di Rilevante Interesse Nazionale (PRIN), Bando 2022", D.D. n. 104/2022, project "COMˆ3D-CREATE", grant No. 2022SMSZZ9.

REFERENCES

[1] Michell, A. G. M. (1904). The limits of economy of material in frame-structures. *The London, Edinburgh, and Dublin Philosophical Magazine and Journal of Science, 8(47), 589-597*

[2] Feng, J., Fu, J., Yao, X., & He, Y. (2022). Triply periodic minimal surface (TPMS) porous structures: from multi-scale design, precise additive manufacturing to multidisciplinary applications. *International Journal of Extreme Manufacturing, 4(2), 022001*

[3] Vidyasagar, A., Krödel, S., Kochmann, D. (2018). Microstructural patterns with tunable mechanical anisotropy obtained by simulating anisotropic spinodal decomposition. *Proceedings of the Royal Society A: Mathematical, Physical and Engineering Sciences, 474, 20180535*

[4] Sanders, E. D., Pereira, A., Aguiló, M. A., & Paulino, G. H. (2018). PolyMat: an efficien Matlab code for multi-material topology optimization. *Structural and Multidisciplinary Optimization, 58, 2727-2759*

[5] Nale, A., Chiozzi, A. (2025). Multiscale topology optimization with embedded TPMS Architected Materials. *International Journal of Mechanical Sciences, (in press).*

[6] Nale, A., Chiozzi, A., Senhora, F.V., and Paulino, G.H. (2025). Large-scale additive manufacturing of optimally-embedded spinodal material architectures. *Additive Manufacturing, 101, 104700*

[7] Bourdin, B. (2001). Filters in topology optimization. *International journal for numerical methods in engineering, 50(9), 2143-2158*

[8] Guest, J. K., Prévost, J. H., & Belytschko, T. (2004). Achieving minimum length scale in topology optimization using nodal design variables and projection functions. *International journal for numerical methods in engineering, 61(2), 238-254*

[9] Bendsøe, M. P. (1989). Optimal shape design as a material distribution problem. *Structural optimization, 1, 193-202*

[10] Bathe, K. J. (1996). Finite element procedures. *Klaus-Jurgen Bathe*

[11] Hassani, B., & Hinton, E. (2012). Homogenization and structural topology optimization: theory, practice and software. *Springer Science & Business Media*

[12] Nocedal, J., & Wright, S. J. (Eds.). (1999). Numerical optimization. *Springer New York*

[13] Bertsekas, D. P. (1997). Nonlinear programming. *Journal of the Operational Research Society, 48(3), 334-334*

[14] Senhora, F. V., Sanders, E. D., & Paulino, G. H. (2022). Optimally-tailored spinodal architected materials for multiscale design and manufacturing. *Advanced Materials, 34(26), 2109304*

[15] Desamanera. La stampa 3D dei Minerali per le grandi dimensioni. *www.desamanera.com*

[16] Binder, K. (1987). Theory of first-orde phase transitions. *Reports on progress in physics, 50(7), 783*

[17] Cahn, J. W., & Hilliard, J. E. (1958). Free energy of a nonuniform system. I. Interfacial free energy. *The Journal of chemical physics, 28(2), 258-267*

[18] Portela, C. M. (2019). Fabrication, Mechanical Characterization, and Modeling of 3D Architected Materials Upon Static and Dynamic Loading. *California Institute of Technology*

[19] Senhora, F. V., Giraldo-Londono, O., Menezes, I. F., & Paulino, G. H. (2020). Topology optimization with local stress constraints: a stress aggregation-free approach. *Structural and Multidisciplinary Optimization, 62, 1639-1668*